Land Use Land Cover Classification using SAR Images and Deep Learning Technique

Internship Report

Submitted in partial fulfillment of the requirements

For the degree of

Bachelor of Technology in Computer Science & Engineering

By

Pranshu Patel	Utsav Patel	Yugma Patel
19BCE191	19BCE200	19BCE204

Guided By

Swati Jain **Preeti Kathiria**

[DEPARTMENT OF COMPUTER SCIENCE & ENGINEERING]

DEPARTMENT OF COMPUTER SCIENCE & ENGINEERING
Ahmedabad 382481

CERTIFICATE

This is to certify that the Internship entitled "**Land Use Land Cover Classification using SAR Images and Deep Learning Techniques**" submitted by Pranshu Patel[19BCE191], Utsav Patel[19BCE200], Yugma Patel[19BCE204], towards the partial fulfillment of the requirements for the degree of Bachelor of Technology in Computer Science and Engineering of Nirma University is the record of work carried out by her under my supervision and guidance. In my opinion, the submitted work has reached a level required for being accepted for examination.

Dr. Swati Jain,
Associate Professor,
Computer Science and Engineering Dept.,
Institute of Technology,
Nirma University,
Ahmedabad

Dr. Madhuri Bhavsar,
HOD and Professor,
Computer Science and Engineering Dept.,
Institute of Technology,
Nirma University,
Ahmedabad

ACKNOWLEDGEMENT

The authors wish to acknowledge the mentors for the project and this work makes ample use of datasets and image data available on NASA-ISRO SAR mission. This project used SNAP toolbox as the primary software for application and Google Colab for model depolyment.

ABSTRACT

To track global environmental change and assess the risk to sustainable livelihoods and development, analysts and decision-makers in government, civil society, business, and finance need the fundamental geospatial data products known as land use/land cover (LULC) maps. High-level, automated geospatial analysis tools are desperately needed to transform these pixels into information that non-geospatial professionals can use. Due to their great spatial, spectral, and temporal resolution, the Sentinel-1 satellites, which were first launched in the middle of 2014, are excellent candidates for LULC mapping. Deep learning innovations and scalable cloud computing now have the analysis capabilities needed to maximise the potential of observations made from satellite photos around the world. Based on a novel, very large dataset of around 5 meter accuracy, we developed and deployed a deep learning segmentation model on Sentinel-1 data to create a LULC map of the selected regions that achieves state-of-the-art accuracy and enables automated LULC mapping from time series observations.

INTRODUCTION

While the majority of scientists who use remote sensing are familiar with passive, optical images from the Sentinel-2 of the European Space Agency, the Moderate Resolution Imaging Spectroradiometer (MODIS), and the Landsat of the U.S. Geological Survey, another type of remote sensing data, Synthetic Aperture Radar, or SAR, is making waves. SAR is an active data gathering method in which a sensor generates its own energy and then measures how much of it is reflected back after coming into contact with the Earth. While reading optical imaging is akin to reading a picture, reading SAR data requires a distinct mental model because the signal responds to surface qualities like structure and wetness instead. Remote sensing and surface mapping of the Earth and other planets both benefit greatly from the use of SAR photographs. The uses for SAR are countless. Topography, oceanography, glaciology, and geology are among examples (for example, terrain discrimination and subsurface imaging). SAR can be used to measure forest height, biomass, and deforestation in forestry. Differential interferometry is used to detect earthquakes and volcanoes. SAR can be used to monitor the stability of civil infrastructure, such as bridges. SAR is helpful in monitoring environmental conditions including oil spills, flooding, urban growth, and military surveillance, including tactical assessment and strategic policy. SAR can be used as inverse SAR by keeping track of a moving target over a long period of time while using a fixed antenna.

1.1 Topic Title

SAR images are extremely useful for both surface mapping of the Earth and other planets as well as for remote sensing. SAR has a plethora of applications. Examples include topography, oceanography, glaciology, and geology (for example, terrain discrimination and subsurface imaging). SAR can be used in forestry to estimate deforestation, biomass, and forest height. Differential interferometry is used to find volcanic eruptions and earthquakes. SAR can be used to keep an eye on the stability of buildings and bridges. Monitoring environmental circumstances, such as oil spills, flooding, urban development, and military surveillance, including tactical evaluation and strategic policy, is made easier with the use of SAR. By tracking a moving target over an extended period of time while utilising a fixed antenna, SAR can be employed as inverse SAR.

1.2 Objectives

A society's social and economic development is completely correlated with its rate of expansion. This is the main justification behind socioeconomic surveys. Datasets from both spatial and non-spatial sources are used in this kind of survey. The planning, management, and monitoring of programmes

at the local, regional, and national levels heavily relies on LULC maps. On the one hand, this type of information aids in a better understanding of land utilisation issues, and on the other, it is crucial in the establishment of the policies and programmes needed for development planning. Monitoring the ongoing pattern of land use/land cover through time is essential for ensuring sustainable development. Authorities involved in urban development must create these planning models in order to accomplish sustainable urban development and stop the haphazard growth of towns and cities. This will allow for the most rational and efficient use of all of the available land. This calls for knowledge about the region's past and contemporary land usage and land cover. We can study the changes in our surroundings and ecosystem thanks to LULC maps. We can create rules and start programmes to safeguard our environment if we have detailed information about the study area's Land Use and Land Cover.

1.3 Problem Statement

Our problem statement is “Land Use Land Cover Classification of Earth’s surface using SAR imaging and Deep Learning techniques.”

Literature Survey

The freely available satellite data has increased the interest of researchers to explore the remote sensing field. The Sentinel-1 C-band SAR system can penetrate radar signals through volumetric objects, providing better and more precise information on land cover changes, and it can operate at any time of day or night. Adrian et al. [12] labelled 13 crops including urban, water and soil with the help of field data and WorldView-3 (WV3) images, Solórzano et al. [13] created 10 land cover features by using Sentinel-2 images, Planet images, VHR (Very High Resolution) images from google earth and also collected field data, Šćepanović et al. [14] has used freely available high resolution CORINE map [15] having 5 land cover features which is mainly generated for European and seven cooperating countries [15]; Mehra et al. [16], Garg et al. [17] and Gargiulo et al, [18] used 4 class labels mostly having urban, water, forest/vegetation as common class. Mehra et al. [16] applied CART (Classification And Regression Tree) classifier on LANDSAT-8 images to create annotated images, although barren land, which is plainly detectable in the Indian region, was not included in their research. The authors of the papers [17] and [18] did not specify the source of their ground-truth data and did not go into great detail about land cover aspects. Emek et al. used one class for building detection which is taken from SpaceNet database. Scepanovic et al. [14] used CORINE land cover map which as a annotated dataset for land cover features with 100 m X 100 m spatial resolution for across the European territory and 20m X 20m for Finland region but like green urban area are included in forest. Most land cover features, such as vegetation, soil, and water bodies, change with time and season, and can also be altered by natural and man-made disasters. These small scale changes can easily be detected by generating a large number of annotated images with the help of high resolution optical images (such as WV3).

Methodology

3.1 Data Acquisition

The SAR data needed for the classification purpose is available on both European Space Agency and Alaska Search Facility websites and we used Sentinel-1 SAR image datasets for the same. We took the images of areas like Ahmedabad, Gandhinagar and some suburbs of Ahmedabad for our main area of classification. On the website, by selecting the area of interest in the map provided, the whole patch covering the area is to be downloaded and there are various forms of Sentinel-1 data having different band properties like L0, L1, L2 and High Resolution Image. We used L1 Single -Look

Complex image for our classification purpose. The raw SAR data of our selected area of desire is shown in Fig. 3.1. Moreover, one can also use more than one images of the same area of different time periods. We used the image when there were some ample amount of different land bifurcations such as lakes, vegetation land, wet land, barren, urban built-up and urban dwellings.

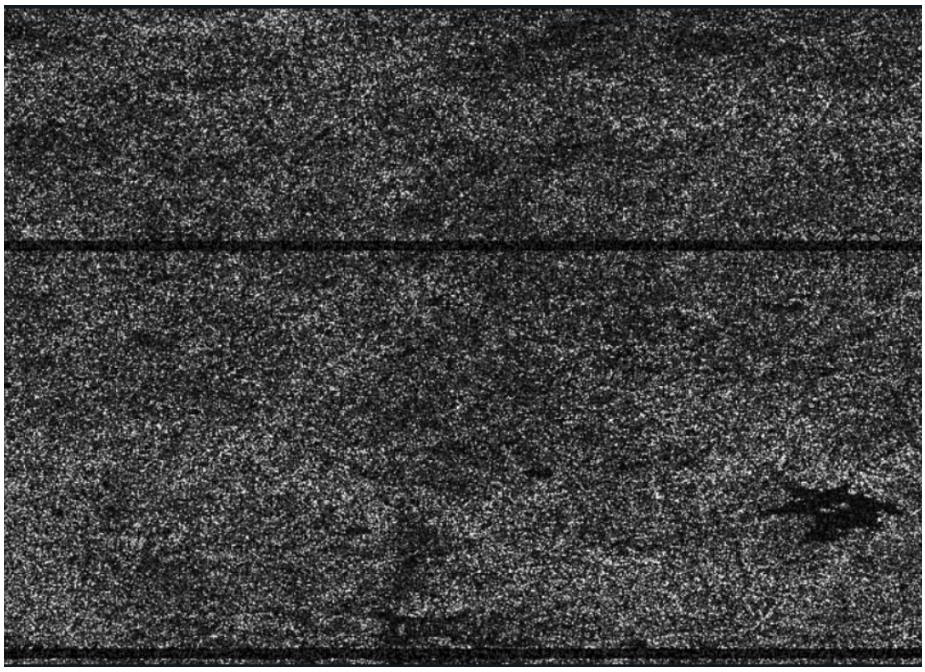

Fig. 3.1 L1 Single-Look Complex image

3.2 Pre-processing

For the pre-processing part, we used the Sentinel Application Platform (SNAP) Sentinel 1 Toolbox which is a graphical user interface (GUI) used for both polarimetric and interferometric processing of SAR data. Start to finish processing includes algorithms for calibration, speckle filtering, coregistration, orthorectification, mosaicking, and data conversion. First of all, after opening the product in SNAP toolbox, we performed Radiometric calibration. As a calibrated measure that takes into consideration the global incidence angle of the image and other sensor-specific properties, radiometric calibration translates the backscatter intensity as it is received by the sensor to the normalised radar cross section (Sigma0). As a result, radar images produced using various dates, sensors, or imaging geometries can be compared. The process of Radiometric Calibration is shown in Fig. 3.2.After that, we used debursting tool to combine the images in proper manner and and it also removes the separation that is earlier seen in the raw image data. Further, we used Thermal Noise removal tool to remove the unidentified dots and lines that are present as noise in the data. By this, the supervised classification that is intended is made more precise and can obtain better classification results from it. After debursting, next step is speckle-filter. Granular patterns are prevalent in many places where a uniform backscatter intensity is anticipated. These salt-and-pepper effects are speckle, which are present in all SAR images and are brought on by various scattering mechanisms that contribute both positively and negatively to the intensity of the backscatter below the pixel resolution. Adaptive speckle filters were developed to improve the quality of the image by reducing random variations while preserving sharp edges. The Lee Sigma filter preserved linear characteristics and crisp boundaries between various surfaces while removing broader regions of comparable backscatter. Due to the undesirable patterns and granular effects that speckle can produce in the outputs of the classification process, this is a crucial prerequisite for the later categorisation of land cover. A robust filtering is required, especially for SAR-based land cover classifications.

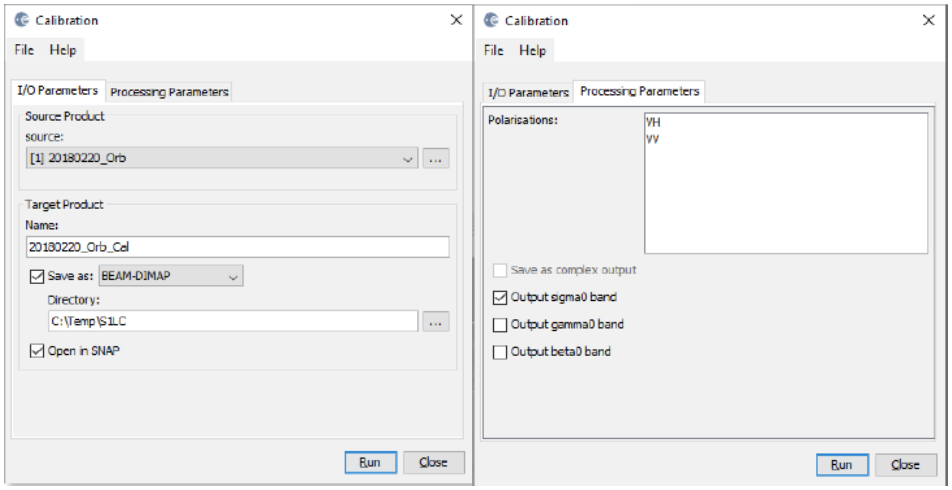

Fig. 3.2. Radiometric calibration

The Terrain Correction tool comes next. By employing a digital elevation model (DEM) to correct SAR geometric errors, Terrain Correction will geocode the image and create a map-projected output. Slant range or ground range geometries are transformed into a map coordinate system through the process of geocoding. Terrain geocoding includes utilising a Digital Elevation Model (DEM) to adjust for foreshortening, layover, and shadow, three common geometric distortions.
This is shown in Fig. 3.3 below.

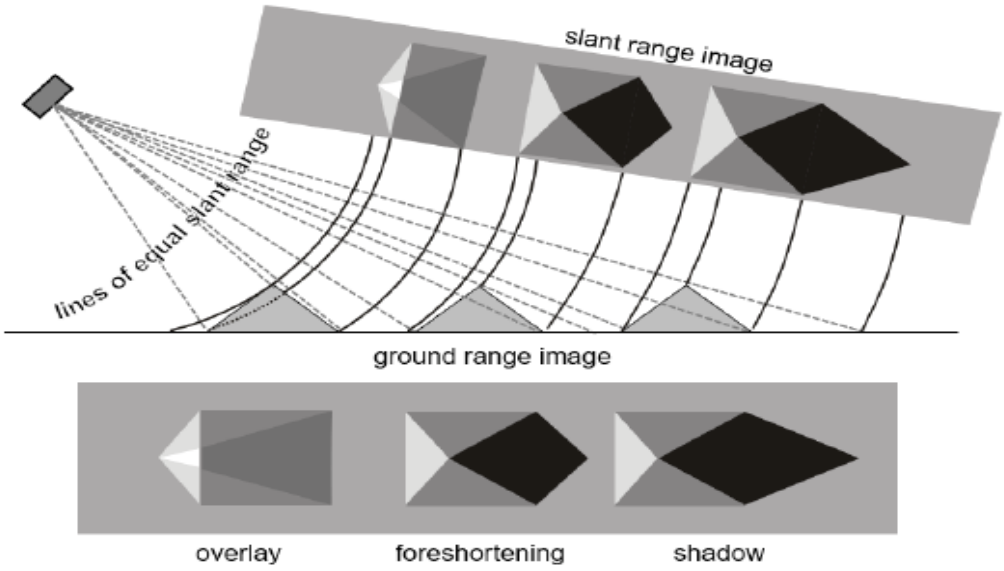

Fig. 3.3. Geometric distortions in radar images

Here in the terrain correction tab more precisely, the Range Doppler Terrain Correction is performed. Under the Range Doppler Operator a series of changes are made from input DEM to selecting WGS84 as Map Projection parameter as shown in Fig. 3.4.

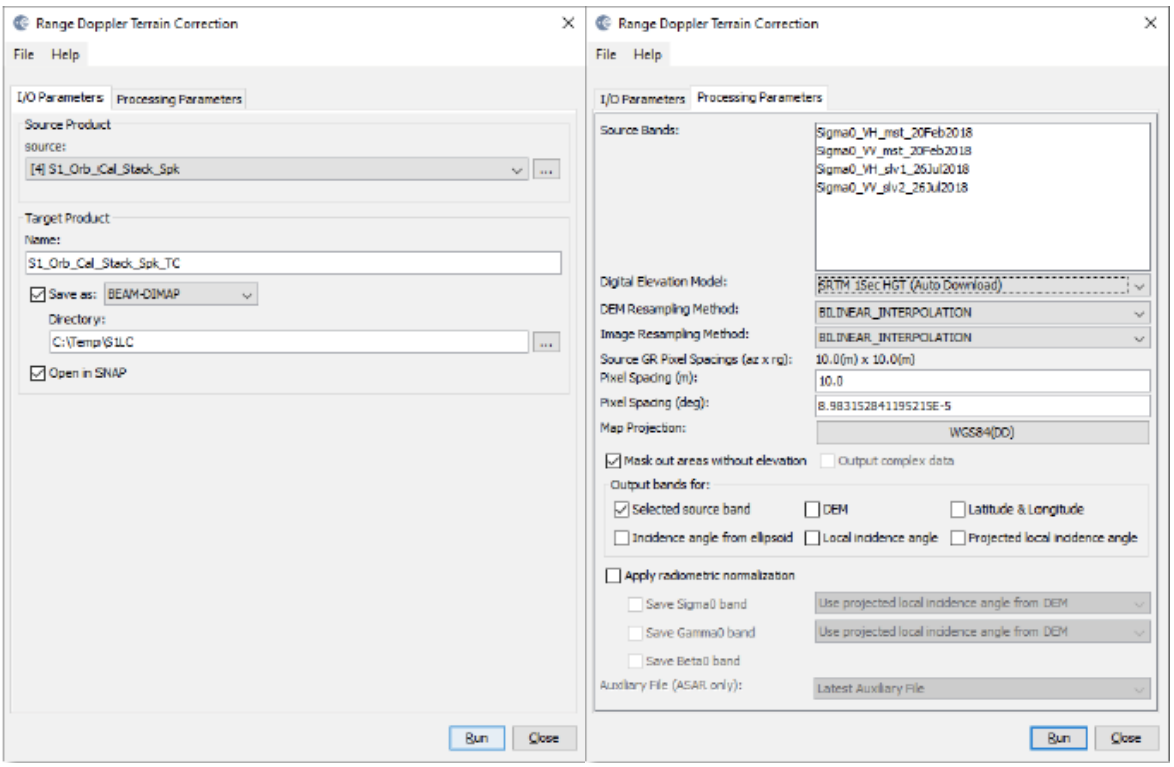

Fig. 3.4. Range Doppler Terrain Correction

3.3 Supervised Classification

The training data for supervised classification must specify the landcover classes and their locations in the final results. There are several ways to accomplish this: importing a shapefile with an attribute column containing the class name; manually digitising vectors that are members of a certain class; importing CSV files that specify a class's geometry.
The supervised classification is basically done in four steps, as shown in Fig. 3.5, the first one being obviously the pre-processing or in this case, the image analysis step. Next comes the Selection of training areas and their digitisation process.

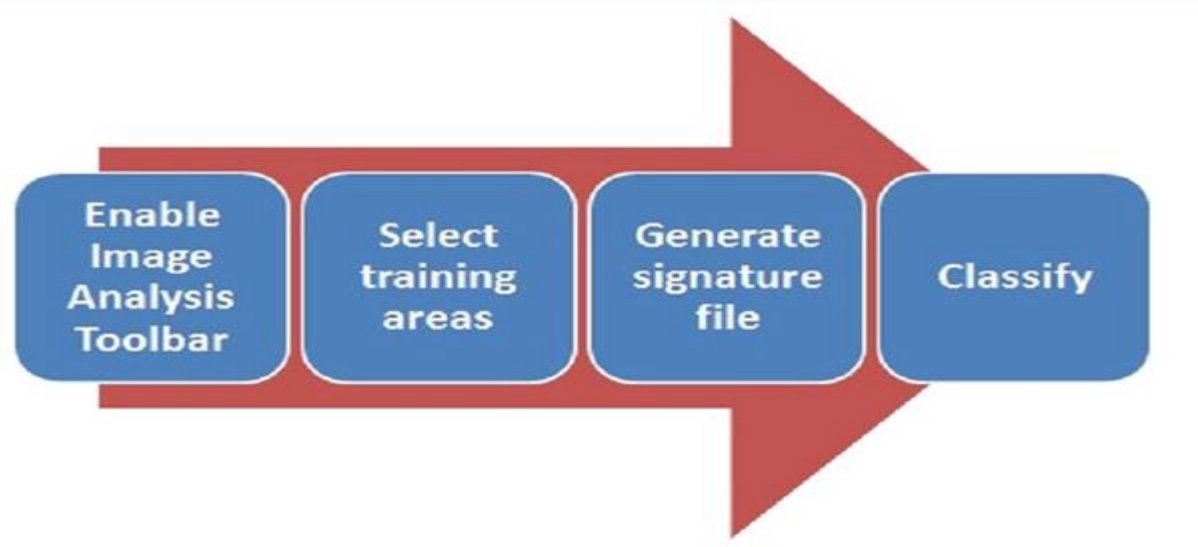

Fig. 3.5. Steps involved in Supervised Classification

Here, in the SNAP toolbox it is also known as the vector data and that can be selected or marked down using vector data containers. Various vector data can be created and for each data the containers

can be drawn using various drawing tools and these vector data are stored in the same SNAP file under the vector data folder as shown in Fig. 3.6 below.

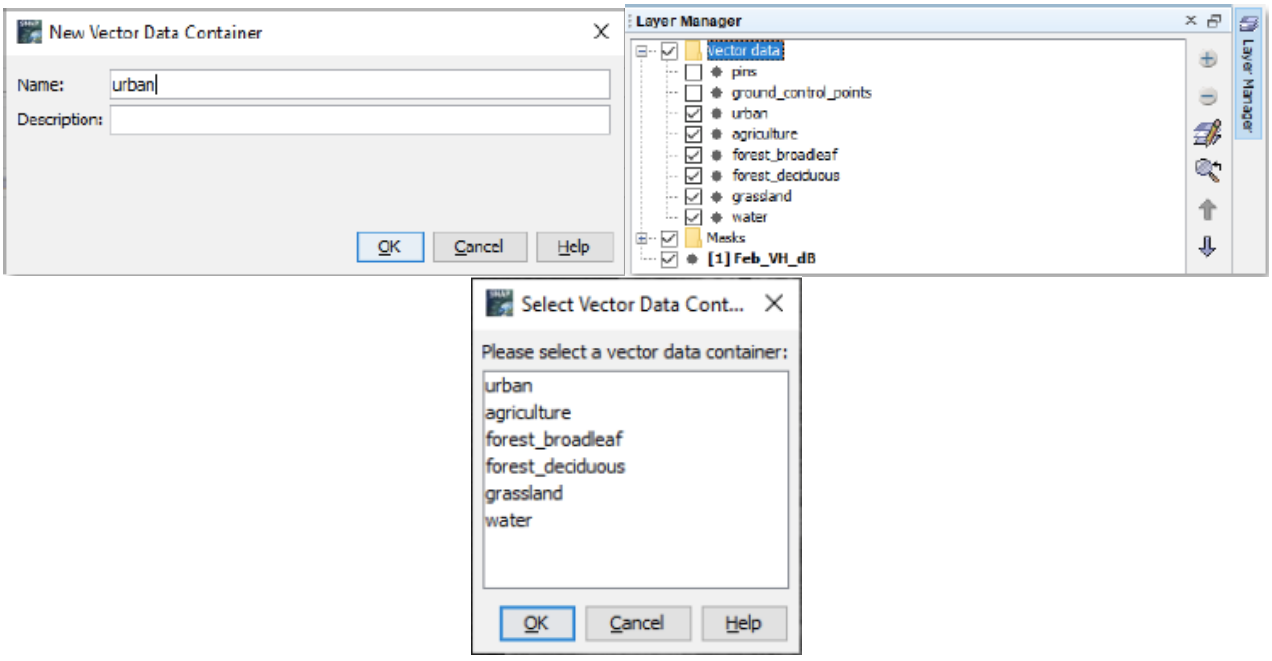

Fig. 3.6. Creation and management of vector containers

In order to use random forest classifier, the number pixels covered in the training samples should more than 5000 for efficient results and vector containers from various areas should be taken for the same. The random forest classifier with 5000 samples and 25 trees is chosen as shown in the Fig. 3.7.

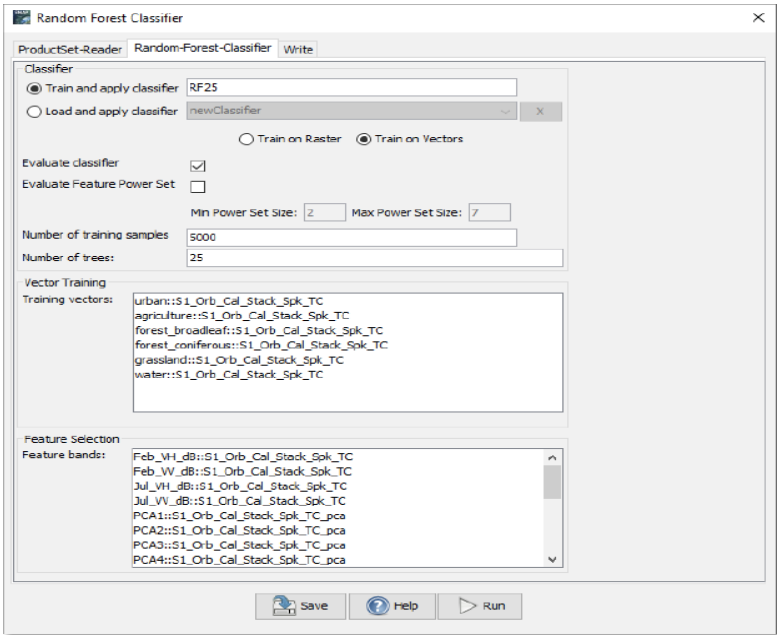

Fig. 3.7. Random Forest - parameters

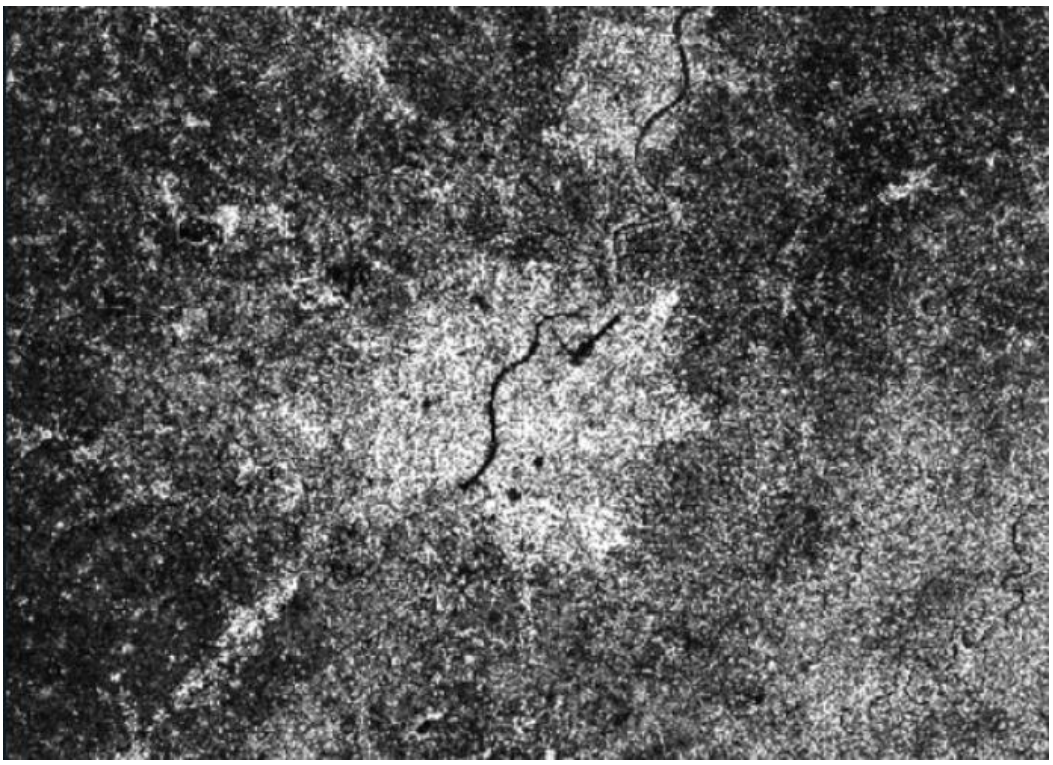

Fig. 3.8 Pre-processed Single Look Complex Image

The Fig. 3.8 shows the transition from raw Single Look Complex data to the useful preprocessed data.The final image with labelled classes obtained using random forest classifier in the SNAP toolbox is shown in Fig. 3.9.

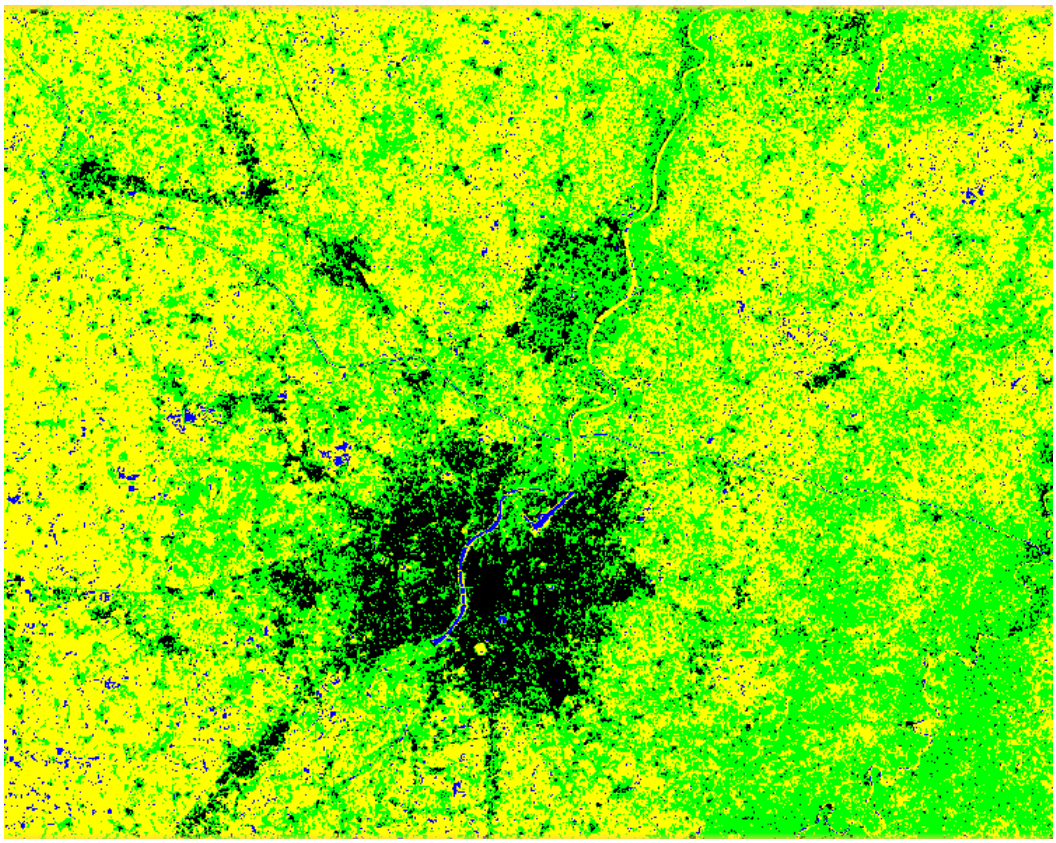

Fig 3.9 Labelled Classes after applying supervised classification using Random Forest Classifier

```
RandomForest classifier newClassifier
Cross Validation
Number of classes = 4
   class 0.0: vegetation
    accuracy = 0.9636 precision = 0.9312 correlation = 0.9145 errorRate = 0.0364
    TruePositives = 3534.0000 FalsePositives = 261.0000 TrueNegatives = 9095.0000 FalseNegatives = 216.0000
   class 1.0: water
    accuracy = 0.9997 precision = 0.9995 correlation = 0.9987 errorRate = 0.0003
    TruePositives = 1853.0000 FalsePositives = 1.0000 TrueNegatives = 11249.0000 FalseNegatives = 3.0000
   class 2.0: urban
    accuracy = 0.9904 precision = 0.9853 correlation = 0.9767 errorRate = 0.0096
    TruePositives = 3679.0000 FalsePositives = 55.0000 TrueNegatives = 9301.0000 FalseNegatives = 71.0000
   class 3.0: barren
    accuracy = 0.9729 precision = 0.9559 correlation = 0.9354 errorRate = 0.0271
    TruePositives = 3559.0000 FalsePositives = 164.0000 TrueNegatives = 9192.0000 FalseNegatives = 191.0000

Using Testing dataset, % correct predictions = 96.3299
Total samples = 26212
RMSE = 0.5298217857692538
Bias = -0.008774607050206162

Distribution:
   class 0.0: vegetation                7500        (28.6128%)
   class 1.0: water                     3712        (14.1615%)
   class 2.0: urban                     7500        (28.6128%)
   class 3.0: barren                    7500        (28.6128%)

Testing feature importance score:
Each feature is perturbed 3 times and the % correct predictions are averaged
The importance score is the original % correct prediction - average
   rank 1   feature 9  : Sigma0_VH_GLCMCorrelationscore: tp=0.0272 accuracy=0.0136 precision=0.0239
   rank 2   feature 6  : Sigma0_VH_Entropy        score: tp=0.0252 accuracy=0.0126 precision=0.0214
   rank 3   feature 7  : Sigma0_VH_GLCMMean       score: tp=0.0138 accuracy=0.0069 precision=0.0117
   rank 4   feature 3  : Sigma0_VH_Homogeneity    score: tp=0.0134 accuracy=0.0067 precision=0.0116
   rank 5   feature 16 : Sigma0_VV_GLCMMean       score: tp=0.0131 accuracy=0.0066 precision=0.0117
   rank 6   feature 17 : Sigma0_VV_GLCMVariance   score: tp=0.0115 accuracy=0.0058 precision=0.0098
   rank 7   feature 21 : Sigma0_VH_db             score: tp=0.0095 accuracy=0.0048 precision=0.0083
   rank 8   feature 5  : Sigma0_VH_MAX            score: tp=0.0091 accuracy=0.0046 precision=0.0080
   rank 9   feature 11 : Sigma0_VV_Dissimilarity  score: tp=0.0083 accuracy=0.0041 precision=0.0071
   rank 10  feature 10 : Sigma0_VV_Contrast       score: tp=0.0078 accuracy=0.0039 precision=0.0068
   rank 11  feature 18 : Sigma0_VV_GLCMCorrelationscore: tp=0.0077 accuracy=0.0038 precision=0.0080
   rank 12  feature 15 : Sigma0_VV_Entropy        score: tp=0.0072 accuracy=0.0036 precision=0.0063
   rank 13  feature 4  : Sigma0_VH_Energy         score: tp=0.0063 accuracy=0.0031 precision=0.0054
   rank 14  feature 12 : Sigma0_VV_Homogeneity    score: tp=0.0058 accuracy=0.0029 precision=0.0053
   rank 15  feature 1  : Sigma0_VH_Contrast       score: tp=0.0049 accuracy=0.0024 precision=0.0043
   rank 16  feature 22 : Sigma0_VV_db             score: tp=0.0045 accuracy=0.0022 precision=0.0039
   rank 17  feature 2  : Sigma0_VH_Dissimilarity  score: tp=0.0045 accuracy=0.0022 precision=0.0040
   rank 18  feature 8  : Sigma0_VH_GLCMVariance   score: tp=0.0036 accuracy=0.0018 precision=0.0032
   rank 19  feature 14 : Sigma0_VV_MAX            score: tp=0.0034 accuracy=0.0017 precision=0.0033
   rank 20  feature 13 : Sigma0_VV_Energy         score: tp=0.0020 accuracy=0.0010 precision=0.0019
   rank 21  feature 20 : Sigma0_VV                score: tp=0.0004 accuracy=0.0002 precision=0.0003
   rank 22  feature 19 : Sigma0_VH                score: tp=0.0002 accuracy=0.0001 precision=0.0001
```

Fig. 3.10 Accuracy and Rank of Bands used for Random Forest Classification

3.4 Model Pre-development

After this, for the model development process, we needed to undergo patchification of the processed data. We created patches of 512 pixels and around 204 equal sized images were formed using the image data. After this, we did image segmentation. The division and collection of the image's homogeneous parts is known as segmentation. The segmentation's outcomes meet the requirements for connectedness, border smoothing, and grey consistency. Spatial cleaning based on measurement space is the traditional segmentation technique. For the categorisation and feature extraction of high-resolution remote sensing images, image segmentation is an essential processing step. We used Edge detection image Segmentation for the same. The edge of the object is represented by discontinuous local picture characteristics, which are the most notable local brightness variations in the image,

including changes to the texture, colour, and grey value. Discontinuities are used to identify edges and accomplish image segmentation goals. This is shown in Fig. 3.11.

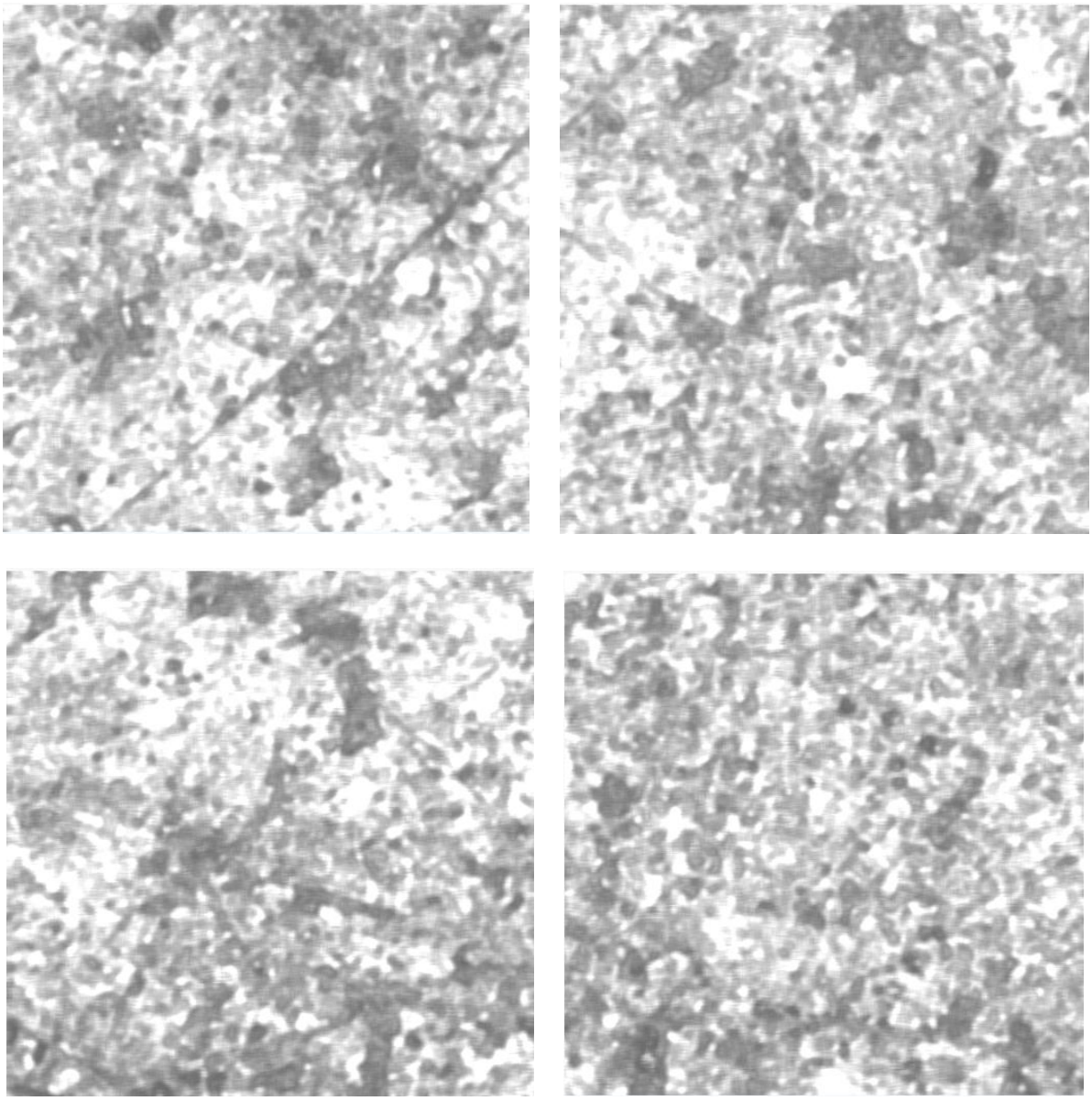

Fig. 3.11 Sample patches of a area used for training data

3.5 Model Development

From beginning, we trained a sizable UNet model. This convolutional neural network architecture, which was first created for the segmentation of biomedical images, has shown to be successful at performing semantic segmentation on satellite photos. With the four classes mentioned above and an additional "no data" class for unlabeled pixels, we construct the segmentation task as a pixel-by-pixel categorical classification problem. In order to correct for class imbalance in the dataset, we used the categorical cross entropy loss function with an inverse-log weighting depending on the percent proportion of each class. We used Adam optimiser for this as it is efficient in sparse noise gradients and can handle it well. Unlabeled parts of the image must be ignored by the model during training since the class weight for unlabeled pixels (i.e., pixels with no data) is wiped out. Each band used in the classification is scaled between 0 and 1 and converted to floating point. By randomly flipping the photos vertically and horizontally, data augmentation is applied, which results in the introduction of more geographic pattern realisations. We use the dropout strategy during training to prevent overfitting by randomly shutting off 20% of the neurons in the UNet in each batch. Until convergence,

the model is trained for 40 epochs at a stepped learning rate that decreases by an order of magnitude once the validation loss reaches a plateau.

3.6 Model Deployment

For the deployment of the UNet model that we trained, we used a 100 km x 100 km tile which incorporates more scenes in it such as barren, built-up, vegetation, water bodies and more. The methodology created was applied on 204 images of size 512 px x 512 px of the greater 100 km tile. The model deployment was accessed with help of Google Colab computer, running upto a RAM of 13 GB and with a storage allocation of around 110 GB depending in the request and user type. With 13 cores of Google Colab working simultaneously and work was completed in 11 hours.

Results and Discussions

On the holdout validation tiles, we get an overall accuracy of 85% for all ten classes. We also calculate the area of each class with 95% confidence error bounds from the error matrix over region. We ran the model for 500 epochs with a batch size of 32.These four areas were picked as the starting point for examination in order to include a range of different geographies and biomes. Water, trees, crops, and built-up areas do exceptionally well across all regions, with user accuracies exceeding 80%, whereas other classes, such as grass, flooded vegetation, and bare terrain, require more work. Significant misunderstanding between shrubs and brush can be seen on both grass and bare land. As the cloud and snow/ice categories are de-weighted during the class weighted mode during model deployment, we do not report accuracy for these categories. The training set's rare classes accurately reflect how uncommon these classes are in general. The confusers make logical sense for classes with lower test scores. For instance, pastures and fallow fields that have similar patterns to cropland but are not actively farmed are the main cause of confusion between grass and crops. Given how challenging it is to describe and discriminate between these two classifications in 5m satellite imagery, confusion between grass and scrub is understandable. We are categorising developed areas aggressively and including characteristics like lawns and parks to avoid confusion between grass and built areas. Though the ground cover may be grass, there are developed places there that serve as useful land uses. The biggest source of confusion for flooded vegetation is crops. Since numerous crops are cultivated on river deltas around the world, there is frequently little difference between these two classes. Similarly, scrub is the primary confuser for bare, and these two classes cross over and gradually merge into one another. We see that, generally speaking, the region's water, trees, crops, and built-up areas are very accurate, although the grass, flooded vegetation, and bare terrain require more work. Given that grassland and scrub/shrub are both primary confusers for bare, it is possible that the model overclassifies scrub/shrub. We can see that the validation dataset's class distribution is not evenly distributed. This mirrors the ambiguity of observations made at the Sentinel-1 scale in the real world.

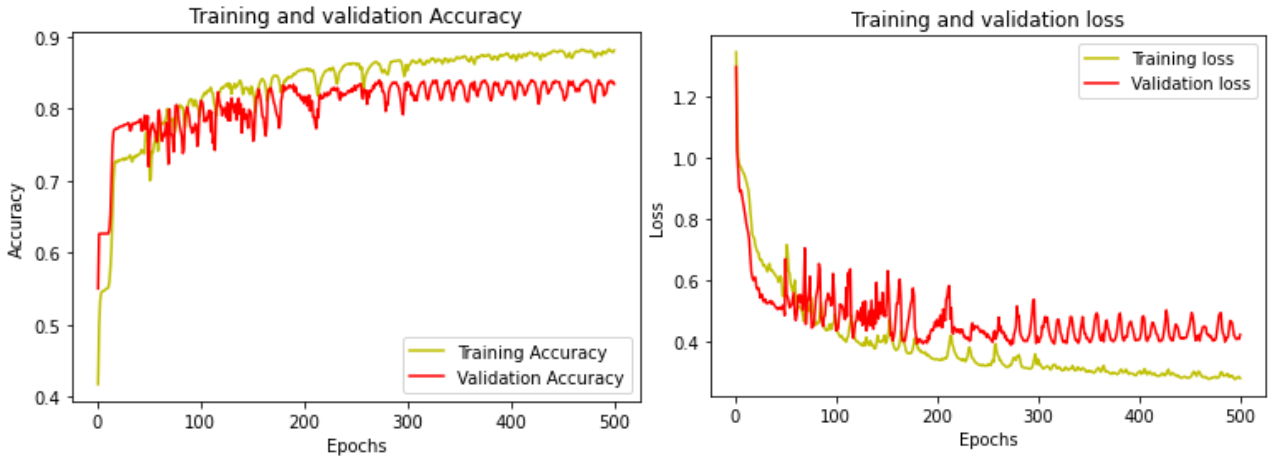

Fig. 3.12 Loss and Accuracy curves for 500 epochs

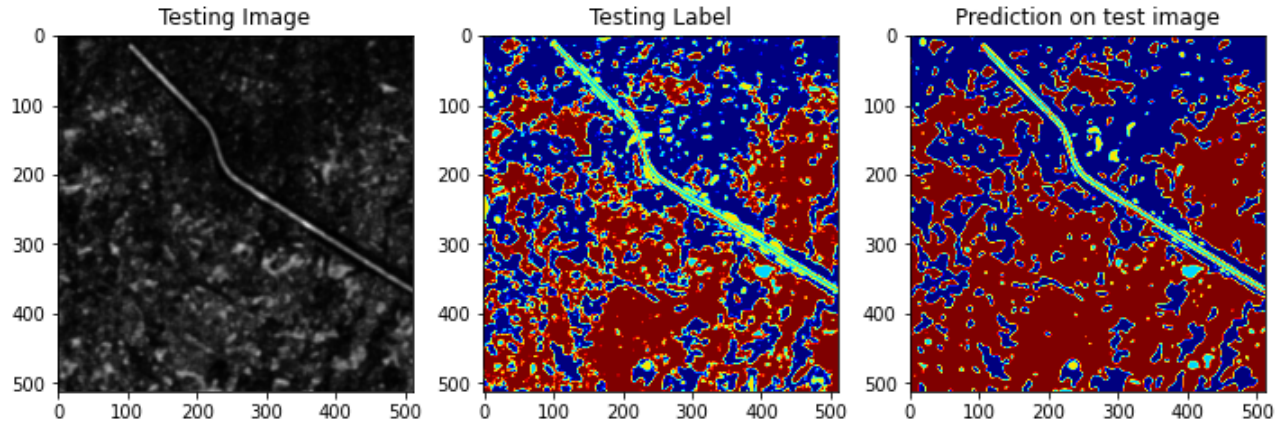

Fig. 3.13 Predicted image for a certain testing image and Label

Conclusions and Future Works

Our findings demonstrate that a globally consistent LULC map at 5m resolution can be produced using a strong training dataset and a deep learning model. Given that the primary confusion factors make intuitive sense and that our model achieves an overall accuracy of 85% across ten classes, we are confident in the validity and use of the global map. There are still a number of exciting possibilities for advancement. Sentinel-1 radiometrically corrected ground range detected (GRD) data, for instance, could be useful for all classes, particularly in separating flooded vegetation from croplands and bare ground from scrub/shrub. Additionally, including time-series data such as assessments of the health of the vegetation over a year could distinguish between grasslands, crops, and scrub and shrub. Additional hand-labeled training data collection to offer more examples of these classes across geographies could increase accuracy for classes that perform poorly (such as grass and flooded vegetation). To enhance model performance and generalisation, we also intend to conduct experiments with other model topologies, class weighting, and other data augmentation strategies. To better understand certain land uses in various regions (such as plantation vs. natural forest, residential vs. commercial built area), we will extend our work to Tier 2 land cover classes.

References

[1] J. R. Anderson, A land use and land cover classification system for use with remote sensor data. US Government Printing Office, 1976, vol. 964.

[2] N. Kumar, S. Yamaç, and A. Velmurugan, "Applications of remote sensing and GIS in natural resource management," Journal of the Andaman Science Association, vol. 20, no. 1, pp. 1–6, 2015.

[3] Y. Xie, W. Dai, Z. Hu, Y. Liu, C. Li, and X. Pu, "A novel convolutional neural network architecture for SAR target recognition," Journal of Sensors, vol. 2019, 2019.

[4] S. Abdikan, F. B. Sanli, M. Ustuner, and F. Calò, "Land cover mapping using sentinel-1 SAR data," in The International Archives of the Photogrammetry, Remote Sensing and Spatial Information Sciences, Volume XLI-B7, 2016 XXIII ISPRS Congress, 2014.

[5] I.-H. Holobâcă, K. Ivan, and M. Alexe, "Extracting built-up areas from Sentinel-1 imagery using land-cover classification and texture analysis," International Journal of Remote Sensing, vol. 40, no. 20, pp. 8054–8069, 2019.

[6] X. Zhu, S. Montazeri, M. Ali, Y. Hua, Y. Wang, L. Mou, Y. Shi, F. Xu, and R. Bamler, "Deep learning meets SAR: concepts, models, pitfalls, and perspectives," IEEE Geoscience and Remote Sensing Magazine (GRSM), 2021.

[7] O. Ronneberger, P. Fischer, and T. Brox, "U-net: Convolutional networks for biomedical image segmentation," in International Conference on Medical image computing and computer-assisted intervention, Springer, 2015, pp. 234–241.

[8] R. A. Emek and N. Demir, "Building detection from sar images using unet deep learning method," The International Archives of Photogrammetry, Remote Sensing and Spatial Information Sciences, vol. 44, pp. 215–218, 2020.

[9] A. Mehra, N. Jain, and H. S. Srivastava, "A novel approach to use semantic segmentation based deep learning networks to classify multi-temporal SAR data," Geocarto International, pp. 1–16, 2020.

[10] M. Cha, R. D. Phillips, P. J. Wolfe, and C. D. Richmond, "Two-stage change detection for synthetic aperture radar," IEEE Trans. Geosci. Remote Sens., vol. 53, no. 12, pp. 6547–6560, Dec. 2015

[11] M. Gong, J. Zhao, J. Liu, Q. Miao, and L. Jiao, "Change detection in synthetic aperture radar images based on deep neural networks," IEEE Trans. Neural Netw. Learn. Syst., vol. 27, no. 1, pp. 125–138, Jan. 2016

[12] J. Adrian, V. Sagan, and M. Maimaitijiang, "Sentinel SAR-optical fusion for crop type mapping using deep learning and Google Earth Engine," ISPRS Journal of Photogrammetry and Remote Sensing, vol. 175, pp. 215–235, 2021.

[13] J. V. Solórzano, J. F. Mas, Y. Gao, and J. A. Gallardo-Cruz, "Land Use Land Cover Classification with U-Net: Advantages of Combining Sentinel-1 and Sentinel-2 Imagery," Remote Sensing, vol. 13, no. 18, p. 3600, 2021.

[14] S. Šćepanović, O. Antropov, P. Laurila, Y. Rauste, V. Ignatenko, and J. Praks, "Wide-Area Land Cover Mapping with Sentinel-1 Imagery using Deep Learning Semantic Segmentation Models," IEEE Journal of Selected Topics in Applied Earth Observations and Remote Sensing, vol. 14, pp. 10 357–10 374, 2021

[15] G. Büttner, "CORINE land cover and land cover change products," in Land use and land cover mapping in Europe, Springer, 2014, pp. 55–74.

[16] A. Mehra, N. Jain, and H. S. Srivastava, “A novel approach to use semantic segmentation based deep learning networks to classify multi-temporal SAR data,” Geocarto International, pp. 1–16, 2020.
[17] R. Garg, A. Kumar, N. Bansal, M. Prateek, and S. Kumar, “Semantic segmentation of PolSAR image data using advanced deep learning model,” Scientific reports, vol. 11, no. 1, pp. 1–18, 2021.
[18] M. Gargiulo, D. A. Dell’Aglio, A. Iodice, D. Riccio, and G. Ruello, “Semantic Segmentation using Deep Learning: A case of study in Albufera Park, Valencia,” in 2019 IEEE International Workshop on Metrology for Agriculture and Forestry (MetroAgriFor), IEEE, 2019, pp. 134–138.

Plagiarism report